

Gyro-based Neural Single Image Deblurring

Heemin Yang¹, Jaesung Rim¹, Seungyong Lee¹,
Seung-Hwan Baek¹, Sunghyun Cho¹

POSTECH¹

{heeminid, jsrim123, leesy, shwbaek, s.cho}@postech.ac.kr

Abstract. In this paper, we present GyroDeblurNet, a novel single image deblurring method that utilizes a gyro sensor to effectively resolve the ill-posedness of image deblurring. The gyro sensor provides valuable information about camera motion during exposure time that can significantly improve deblurring quality. However, effectively exploiting real-world gyro data is challenging due to significant errors from various sources including sensor noise, the disparity between the positions of a camera module and a gyro sensor, the absence of translational motion information, and moving objects whose motions cannot be captured by a gyro sensor. To handle gyro error, GyroDeblurNet is equipped with two novel neural network blocks: a gyro refinement block and a gyro deblurring block. The gyro refinement block refines the error-ridden gyro data using the blur information from the input image. On the other hand, the gyro deblurring block removes blur from the input image using the refined gyro data and further compensates for gyro error by leveraging the blur information from the input image. For training a neural network with erroneous gyro data, we propose a training strategy based on the curriculum learning. We also introduce a novel gyro data embedding scheme to represent real-world intricate camera shakes. Finally, we present a synthetic dataset and a real dataset for the training and evaluation of gyro-based single image deblurring. Our experiments demonstrate that our approach achieves state-of-the-art deblurring quality by effectively utilizing erroneous gyro data.

1 Introduction

Blur caused by camera shakes severely degrades image quality as well as the performance of various computer vision tasks such as classification, object detection, and semantic segmentation. To overcome the image degradation caused by blur, single image deblurring has been extensively studied for decades [6, 12, 14, 17, 32, 48, 52]. Recently, various DNN-based approaches have been proposed and have shown significant performance improvements over classical approaches [4, 5, 23, 24, 31, 44, 51, 53]. Nonetheless, they still fail on images with large blur due to the severe ill-posedness of deblurring, i.e., multiple different blur trajectories could lead to similar-looking blurry images.

To address the ill-posedness, several attempts have been made to exploit gyro sensors with which most smartphones are nowadays equipped. As gyro

data are correlated with motion of the camera mounted on a smartphone, classical approaches based on blur models use gyro data to guide blur kernel estimation [11, 14, 17, 29, 40, 41]. However, their performances are limited by their restrictive blur models that cannot effectively handle noise, nonlinear camera response functions, saturated pixels, moving objects, and so on. With the advance of deep learning, DNN-based approaches have also been proposed to exploit gyro sensors [16, 25, 30]. Thanks to the remarkable capability of DNNs and gyro sensors, they show better performance compared to classical gyro-based approaches and recent DNN-based approaches without gyro sensors.

However, recent DNN-based approaches that utilize gyro data are still limited in handling real-world blurred images. These approaches assume that the gyro data can accurately represent the blur in the blurred image, but this assumption does not hold in practice. First, gyro data from mobile devices such as smartphones usually have a significant amount of noise caused by various sources [10, 17, 19]. Second, gyro sensors measure the angular velocity around their center. Thus, to exploit gyro sensors, the recent gyro-based methods assume that the gyro sensor and the camera share the same center, and the camera is shaken only by rotational motions. However, in practice, the positions of the camera and the gyro sensor are different, and the camera shakes are caused by more complex motions. Third, real-world blurred images may have moving objects with different blur trajectories that cannot be captured by gyro sensors. All these factors make the motion information encoded in the gyro data inconsistent with the blur in the blurred image, and make it difficult to exploit the gyro data in real-world image deblurring. In this paper, we refer to such inconsistency between the gyro data and blur as *gyro error*.

In this paper, we propose *GyroDeblurNet*, a novel gyro-based single image deblurring approach that can produce high-quality deblurring results in the presence of gyro error. To address the gyro error, GyroDeblurNet adopts a carefully designed network architecture that contains a novel gyro refinement block and a novel gyro deblurring block. The gyro refinement block refines gyro data with error using the blur information in the input image. On the other hand, the gyro deblurring block removes blur in the input image using the refined gyro data. To further compensate for gyro error, the gyro deblurring block also exploits the blur information in the input image as well as the input gyro data. Despite the proposed blocks, training a neural network with erroneous gyro data is difficult as the network could be trained to simply ignore the input gyro data. To resolve this issue, we also propose a curriculum-learning-based training strategy [2].

To handle complex real-world camera shakes, we also present the camera motion field, a novel gyro data embedding scheme that can represent complex camera motions. Real-world blurry images often exhibit complex blur trajectories due to random camera shakes, which often occur when shooting a still shot with a long exposure time. Nonetheless, recent gyro-based approaches [16, 25, 30] assume smooth camera motions and represent camera motions using one or two motion vector per pixel or a couple of homographies for the entire image, which leads to low-quality deblurring results. To resolve this issue, our camera motion

field is designed to represent complex camera motions using multiple vectors per pixel while maintaining a comparable memory footprint exploiting the spatially smooth nature of camera shakes.

For the training and evaluation of gyro-based deblurring, previous methods [16, 25, 30] rely on synthetic datasets. However, these datasets do not accurately reflect the noise and blur in real-world blurred images as shown by Rim *et al.* [35]. Additionally, their gyro data do not reflect real-world camera shakes that occur when capturing still-shot images either. Gyro data of previous methods were generated by random sampling [54] or obtained from the Visual-Inertial dataset [38]. However, the Visual-Inertial dataset is originally developed for visual odometry and SLAM, so its camera motions are collected from constantly moving cameras, which differ from camera shakes of still-shot images.

For training and evaluation of gyro-based deblurring for real-world blurred images, we propose two datasets: *GyroBlur-Synth* and *GyroBlur-Real*. GyroBlur-Synth is a synthetic dataset for both training and evaluation. The dataset consists of sharp and blurred image pairs with their corresponding gyro data. The gyro data are acquired from a smartphone device to reflect the real-world camera shakes. The blurred images are synthetically generated using the acquired gyro data and the blur synthesis process of RSBlur [34] for realistic blur. GyroBlur-Real is a real-world blur dataset for qualitative evaluation with no ground-truth sharp images. GyroBlur-Real provides 100 real-world blurred images paired with gyro data collected from a smartphone.

We validate the performance of GyroDeblurNet on both synthetic and real-world datasets. Our experiments demonstrate that GyroDeblurNet clearly outperforms state-of-the-art deblurring methods both quantitatively and qualitatively. Our contributions can be summarized as follows:

- We propose a novel gyro-based single image deblurring approach, *GyroDeblurNet*. Extensive quantitative and qualitative evaluations show that GyroDeblurNet outperforms existing single image deblurring methods.
- To handle gyro error, we introduce a carefully designed network equipped with a novel gyro refinement block and a novel gyro deblurring block. We also develop a novel gyro data embedding scheme to represent complex camera shakes and propose a curriculum learning-based training scheme.
- We present synthetic and real image-gyro paired datasets with realistic camera motions, GyroBlur-Synth and GyroBlur-Real, for training and evaluating gyro-based single image deblurring methods.

2 Related Work

A variety of DNN-based single image deblurring approaches have recently been proposed [4, 5, 21, 23, 24, 31, 44, 45, 47, 51, 53]. To push the limit of single image deblurring, they introduce various network architectures and training schemes. Nevertheless, single image deblurring is still a challenging problem due to its high ill-posedness, and they still fail on images with large blur.

To resolve the ill-posedness of deblurring, there have been attempts to leverage inertial measurement sensors such as the gyro sensor and accelerometer as they provide valuable information on the rotational and translational motion of a camera, respectively. Joshi *et al.* [17] and Hu *et al.* [14] exploit the gyro sensor and accelerometer to estimate spatially-varying blur kernels. On the other hand, Park and Levoy [11] and Mustaniemi *et al.* [29] use only the gyro sensor to estimate blur kernels, because blur kernel estimation using accelerometer measurements requires estimating the depth of a scene, the device orientation to compensate the gravity effect, and the initial velocity of the device, which is often error-prone in practice. Moreover, rotational motion can be assumed as the dominant factor of camera shake blur as discussed by Whyte *et al.* [48].

In the deep learning era, there have been a few works that exploit gyro data. Mustaniemi *et al.* [30] propose a DNN-based approach that uses gyro data for the first time. They introduce a U-Net-based architecture [36] that takes a concatenation of a blurred image and the gyro data as input, which is also adopted by Lee *et al.* later [25]. Ji *et al.* [16] present a deformable-convolution-based network module for handling gyro data, which computes deformable convolution offsets from input gyro data to transform convolution filters according to the blur direction. However, these methods assume that the gyro data is accurate, neglecting potential errors. Moreover, they assume smooth camera motions and model camera motions using a motion vector field consisting of either one [30] or two motion vectors [16] per pixel, or a couple of homographies [25] representing the beginning and end position of the camera during the exposure time. Unfortunately, such restrictive assumptions do not hold for real-world blurred images with complex camera shakes as discussed in Sec. 1.

Utilizing gyro data by converting it into the form of motion vectors for single image deblurring can be considered as a non-blind deconvolution approach. While non-blind deconvolution methods have been studied for decades [18, 22, 26, 33, 49], they are not robust to blur kernel errors and produce unsatisfactory results with erroneous blur kernels. To overcome such limitation, several works adopted hand-crafted priors such as sparse prior [15], hyper-Laplacian prior [22, 46] and deep residual prior [43]. However, they may fail to utilize erroneous blur kernels where such prior assumptions do not hold.

3 GyroDeblurNet

The goal of GyroDeblurNet is to estimate a sharp deblurred image S from an input blurred image B and its corresponding gyro data G possibly with large errors. Specifically, we define G as a sequence of gyro data such that $G = \{g_0, \dots, g_{T-1}\}$, where g_t is the t -th gyro data consisting of three angular velocities during the exposure time. T is the number of gyro data, which is proportional to the exposure time. For example, $T = 20$ if the exposure time is 0.1 seconds, and the sampling rate of the gyro sensor is 200 Hz. Instead of directly using G , we devise a novel gyro data embedding scheme named camera motion field to effectively handle complex camera shakes of an arbitrary expo-

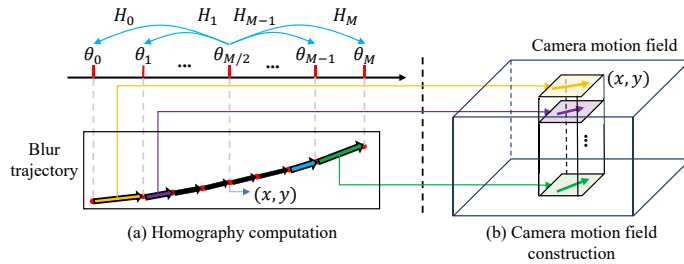


Fig. 1: Camera motion field construction. (a) Computing homography and warped pixel coordinates. (b) Constructing camera motion field by stacking motion vectors.

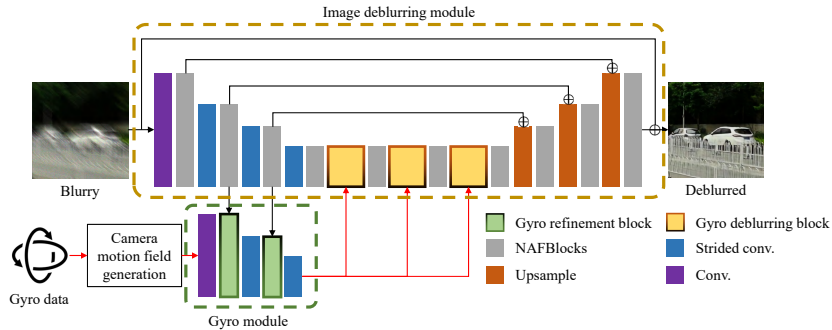


Fig. 2: Network architecture of GyroDeblurNet.

sure duration. In the rest of this section, we explain the gyro data embedding scheme based on the camera motion field, network architecture, and training strategy of GyroDeblurNet in detail.

3.1 Gyro Data Embedding

GyroDeblurNet first converts input gyro data sequence G into a camera motion field \mathcal{V} before feeding it into the subsequent neural network to handle temporally complex camera shakes of an arbitrary length T . The conversion process is illustrated in Fig. 1. Our camera motion field has a fixed channel size $2M$ where M is a hyperparameter, regardless of the length of the input gyro data to allow it to be fed to convolutional neural networks. To achieve this, we first resample the input gyro data sequence G of an arbitrary length T to $M + 1$ samples using cubic-spline interpolation. We denote the resampled sequence as $G' = \{g'_0, \dots, g'_M\}$ where g'_m is a resampled gyro sample. The hyperparameter M is set to an even number so that we have the same number of gyro data before and after the temporal center of the exposure duration.

Then, assuming that the camera and the gyro shares the same center and there exists neither off-center rotational nor translational motions, we integrate the angular velocities and obtain $M + 1$ camera orientations θ_m , where $m = 0, \dots, M$, including the camera orientations at the beginning and end of the exposure. Note that, despite our restrictive assumption on the camera motion,

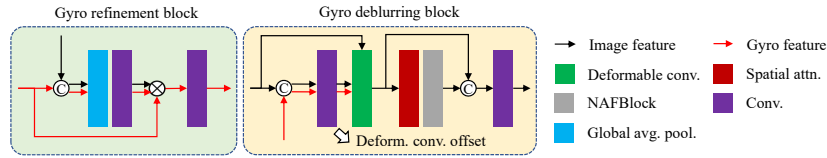


Fig. 3: Detailed architectures of the gyro refinement block and gyro deblurring block.

GyroDeblurNet can successfully perform deblurring thanks to its robustness to gyro errors. For each θ_m , we compute a homography H_m as $H_m = KR(\theta_m)K^{-1}$ where K is the camera intrinsic matrix and $R(\theta_m)$ is the rotation matrix corresponding to θ_m . Based on the camera orientation that we chose as a reference, there can be multiple sets of homography H_m each of which leads to shifted vector field. To prevent unnecessary shift after deblurring, we assume $\theta_{M/2}$ at the temporal center to be $(0, 0, 0)$ so that $H_{M/2}$ is an identity matrix when computing θ_m .

Finally, from the obtained homographies, we compute a camera motion field \mathcal{V} , which illustrates how each pixel is blurred. Specifically, we define a camera motion field \mathcal{V} as a tensor of size $W/s \times H/s \times 2M$ where W and H are the width and height of the input blurred image, and s is a scaling factor. Then, at each spatial position (x, y) in \mathcal{V} , we compute the warped coordinates of (x, y) by H_m for all m and compute the difference between temporally consecutive coordinates to obtain M motion guidance vectors at each position. By stacking the vectors for all the spatial positions, we construct \mathcal{V} . In our experiments, we set $M = 8$ and $s = 2$.

Our camera motion field is motivated by the blur field proposed by Mustaniemi *et al.* [30] and the motion guidance vector (MGV) field introduced by Ji *et al.* [16]. Unlike previous methods that rely on only one or two vectors to represent camera shakes at each pixel, our camera motion field offers a more sophisticated representation. By adjusting the hyperparameter M , it can effectively capture temporally intricate camera shake patterns. Furthermore, our approach leverages the spatial smoothness of camera shakes, utilizing the hyperparameter s . As a result, it can provide a detailed representation of complex motions while maintaining a comparable memory footprint.

3.2 Network Architecture

The network architecture of GyroDeblurNet is illustrated in Fig. 2. GyroDeblurNet takes a blurred image B and a camera motion field \mathcal{V} as input and estimates a deblurred image S . The network consists of two modules: an image deblurring module and a gyro module. The image deblurring module takes a blurred image B and performs deblurring with the aid of gyro data. It then produces a residual R that is added back to B to produce S . The image deblurring module adopts a U-Net architecture [36] and the NAFBlock [4] as its basic building block. The image deblurring module adopts gyro deblurring blocks in its bottleneck to perform deblurring using gyro features from the gyro module.

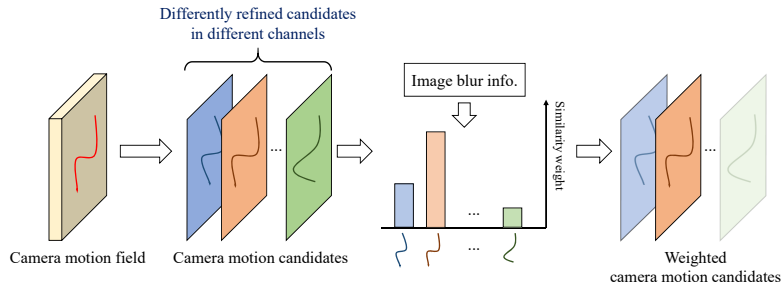


Fig. 4: The input camera motion field passes a convolutional layer to produce differently refined camera motion candidates in different channels. The candidates are then weighted by computing similarity with the blur information of the blurred image.

On the other hand, the gyro module takes a camera motion field \mathcal{V} and refines it with the aid of image features from the image deblurring module. The gyro module consists of a convolution layer to embed an input camera motion field \mathcal{V} into the feature space, and gyro refinement blocks. The gyro refinement blocks refine gyro features with the aid of image features from the encoder of the image deblurring module. The gyro module progressively refines gyro features through gyro refinement blocks and strided convolution layers, and obtains a gyro feature of the same spatial size as the feature maps of the bottleneck in the image deblurring module. In the following, the gyro refinement block and the gyro deblurring block, which are the two key components of GyroDeblurNet, are explained in detail. For a detailed network architecture including feature dimensions, refer to the supplementary material.

Gyro refinement block The structure of the gyro refinement block is illustrated in Fig. 3. The gyro refinement block takes a gyro feature computed from the input camera motion field \mathcal{V} as input. Then, it refines the gyro feature using the channel attention mechanism [13] with the aid of an image feature from the encoder of the image deblurring module. Specifically, the gyro refinement block takes an image feature from the image deblurring module as an additional input, and concatenates it with the input gyro feature. It then computes channel-wise attention weights through global average pooling and 1×1 convolution layers, and refines the gyro feature using the obtained channel-wise attention weights. Finally, it applies a convolution layer to further refine the gyro feature.

The intuition behind the refinement process by the gyro refinement block is illustrated in Fig. 4. The camera motion information in the input camera motion field \mathcal{V} may contain a significant amount of error. From such an erroneous camera motion information, the convolution layer at the beginning of the gyro module produces a gyro feature consisting of multiple camera motion candidates at different channels by introducing different perturbations to the input camera motion information. Then, the gyro refinement block adaptively selects the channels of the gyro feature that are consistent with the blur information encoded in the image feature using the channel attention weights computed from both gyro and image features [13].

Gyro deblurring block The structure of the gyro deblurring block is shown in Fig. 3. The gyro deblurring block performs deblurring of the image feature with the gyro feature from the gyro module. The input image B may have spatially-variant blur caused by camera shakes and moving objects. To effectively remove such spatially-varying blur in the image feature, the gyro deblurring block adopts the deformable convolution operation [7, 55], whose offsets are computed based on both image and gyro features. As the gyro feature provides accurately refined information on the camera shakes, and the image feature provides information on the blur in B including object motion blur, the gyro deblurring block can successfully handle both camera shakes, and object motion blur.

To further remove the remaining spatially-variant blur in the deblurred image feature, the gyro deblurring block applies a spatial attention block to the deblurred image feature following Xu *et al.* [50]. The deblurred feature is then further refined through a NAFBlock and a convolution layer. While deformable convolution has also been employed by EggNet [16] to deblur images using gyro data, EggNet applies it without accounting for real-world gyro errors. This oversight leads to subpar results for real-world images, as will be shown in Sec. 5. In contrast, our approach incorporates network modules, a training strategy, and data specifically designed to accommodate real-world gyro errors.

3.3 Training Strategy

Despite the gyro refinement block and gyro deblurring block, it is still challenging to train a deblurring network with erroneous gyro data. Naïvely training the network with erroneous gyro data can lead the network to ignore the gyro data and simply rely only on the blur information in the blurred image. Thus, to train our network to fully utilize input gyro data, we introduce a training strategy based on curriculum learning [2], which has shown superior performance in various learning-based approaches that deal with erroneous data [37, 39, 42].

Our training strategy initially trains the network with error-free gyro data, and gradually increases error in the training data. To this end, we first assume that for each blurred image B , its corresponding error-free gyro data G_{GT} is given as well as its ground-truth sharp image S_{GT} . From G_{GT} , we compute a noise-free camera motion field \mathcal{V}_{clean} and a noisy camera motion field \mathcal{V}_{noisy} . We generate \mathcal{V}_{noisy} by randomly perturbing the rotational center and adding noise to the gyro data G_{GT} . We then compute a blended camera motion field $\mathcal{V}_\alpha = (1 - \alpha) \cdot \mathcal{V}_{clean} + \alpha \cdot \mathcal{V}_{noisy}$ where α is a blending parameter. Finally, we train our network with a PSNR loss [3, 4], which is defined as:

$$\mathcal{L}_{PSNR} = 10 \cdot \log_{10}(\|f(B, \mathcal{V}_\alpha) - S_{GT}\|^2 + \epsilon) \quad (1)$$

where $f(B, \mathcal{V}_\alpha)$ represents a deblurred output of GyroDeblurNet and ϵ is a small constant to prevent the negative infinity, which is set to $1e-8$ in our experiments. We initially set α to 0, and gradually increase it to 1 during training. For more details including the noisy camera motion field generation and the scheduling of α , refer to the supplementary material.



Fig. 5: Examples of the GyroBlur-Synth and GyroBlur-Real datasets. In (a), the top and bottom rows show ground-truth images and the corresponding blurry images, respectively.

4 GyroBlur Dataset

4.1 GyroBlur-Synth

GyroBlur-Synth provides 14,600 and 640 synthetically blurred images of size 720×1280 for the training and test sets. The dataset also provides ground-truth sharp images, ground-truth clean gyro data. To faithfully mimic real-world blurred images, the dataset covers various sources of image degradation, such as camera shakes, moving objects, noise, and saturation. The dataset also includes gyro error data to produce realistic erroneous gyro data from the clean gyro data. Fig. 5 (a) shows examples of GyroBlur-Synth.

To build a dataset with realistic camera motions, we implemented an Android application that records gyro data on a mobile phone. We used a Samsung Galaxy S22 smartphone for collecting gyro data with the sampling rate of 200 Hz. We collected two sequences of gyro data for generating training and test datasets with realistic hand-shake motions. The gyro data sequences are recorded for 195 sec. and 60 sec., and have 39,116 and 12,065 samples, respectively. We then used the gyro data to synthesize blurry images. To this end, we used sharp frames of the 4KRD dataset [8]. To generate a blurry image, we first randomly sampled a sequence of 10 consecutive gyro data corresponding to the exposure time of $1/20$ seconds. We then interpolated them by eight times to synthesize a continuous blur trajectory, and computed homographies from the interpolated gyro data. Finally, we warped the sharp image using the homographies, and blended them to obtain a blurry image.

To create synthetic blurred images with moving objects that have different blur trajectories, we used a simple method. We select a single instance from the COCO dataset [27] and assume it moves at a constant speed in a blurry image. We randomly choose its position and the direction and speed of motion. We then add the object to the warped sharp images before blending them during the blur synthesis process described earlier. This method may seem simple, but our experiment shows that it helps train our model to better handle spatially-variant motion blur from moving objects.

To reflect real-world noise and saturated pixels, we also adopt the blur synthesis pipeline of RSBlur [34]. Specifically, we synthesize blur in the linear sRGB space following the aforementioned process. Then, we synthesize saturated pixels, convert the image into the camera RAW space, synthesize noise, and convert the noisy RAW image to the linear sRGB image. We refer the readers to [34]

for the detailed blur synthesis process. The blur synthesis pipeline of RSBlur requires camera parameters such as a color correction matrix and a noise distribution. To this end, we use the camera parameters of a Samsung Galaxy S22 ultra-wide camera, and the noise distribution estimated from it.

The gyro error data includes gyro noise and randomly perturbed rotation centers for generating noisy camera motion fields. To obtain realistic gyro noise, we measured the gyro noise distribution from a stationary smartphone (Samsung Galaxy S22) placed on a table. Gyro noise is modeled as a Gaussian distribution for each rotation axis independently. For more details on the dataset, we refer the readers to the supplementary material.

Our synthetic dataset generation approach requires minimal device-specific information, including a small amount of gyro data sequences and parameters. This approach minimizes the need for laborious manual data collection. Specifically, we can collect a sufficient amount of gyro data by holding a smartphone in hand only for a couple of minutes, and by placing a smartphone on a table only for a few seconds. The camera parameters required for the RSBlur pipeline can also be easily obtained by a simple calibration process with a couple of images captured by a target camera. Note also that our synthetic dataset approach process does not explicitly model the relative position of the gyro sensor with respect to the camera module, which is information that is hard to access. Instead, our approach implicitly models it as part of rotational center error. Despite this, our experiments show that our approach can effectively remove blur.

4.2 GyroBlur-Real

GyroBlur-Real provides 100 real-world blurry images and their corresponding gyro data for qualitative evaluation. The dataset was collected using a Samsung Galaxy S22. The blurry images are of size 4080×3060 , and provided in both raw DNG and JPEG formats. The dataset also provides metadata such as timestamps of the images and gyro data, camera intrinsic parameters, exposure times and ISO parameters. Fig. 5 (b) shows examples of GyroBlur-Real.

5 Experiments

For evaluation, we implemented our network using PyTorch. We trained our network on randomly cropped 256×256 image patches from the GyroBlur-Synth dataset for 300 epochs with a batch size of 16. We used the Adam optimizer [20] with $\beta_1 = 0.9$ and $\beta_2 = 0.999$. The learning rate was initially set to 0.0001 and reduced to $1e-7$ using the cosine annealing scheduler [28]. We measured the computation times of all the models on a GeForce RTX 3090 GPU.

One well-known issue in using gyro data is that the timestamps of the gyro sensor and the camera are not synchronized. Fortunately, several approaches that can successfully synchronize the gyro sensor and camera have been proposed [9]. Thus, in our work, we assume that the input gyro data are already synchronized for the exposure time of the input image. GyroBlur-Real dataset was collected using an open-source Android application [1] that supports synchronization between the gyro and camera based on gyro-based clock synchronization [9].

Table 1: Quantitative comparison on the test of GyroBlur-Synth. The inference times of the models that use gyro data include both gyro data embedding (e.g., camera motion field construction) and deblurring processes.

| Gyro | Models | PSNR | SSIM | Param. (M) | MACs (G) | Time (s) |
|------|------------------|-------|--------|------------|----------|----------|
| X | MPRNet [51] | 25.03 | 0.7081 | 20.13 | 10927 | 0.998 |
| | NAFNet [3] | 25.06 | 0.7085 | 17.11 | 227 | 0.106 |
| | Uformer-B [47] | 25.72 | 0.7334 | 50.88 | 2143 | 1.061 |
| | Stripformer [45] | 25.93 | 0.7398 | 19.71 | 2397 | 1.367 |
| | FFTformer [21] | 26.01 | 0.7481 | 16.56 | 1894 | 1.879 |
| | DeepGyro [30] | 23.78 | 0.6649 | 31.03 | 769 | 0.068 |
| O | EggNet [16] | 25.49 | 0.7266 | 6.34 | 1102 | 0.071 |
| | Ours | 27.28 | 0.7803 | 16.31 | 262 | 0.130 |

In the remainder of this section, we present the performance evaluation of GyroDeblurNet. We evaluate the performance of our method using the test set of GyroBlur-Synth and GyroBlur-Real. Additional experiments and examples including visualization of the effect of gyro refinement and an analysis on the robustness to gyro errors are included in the supplementary material.

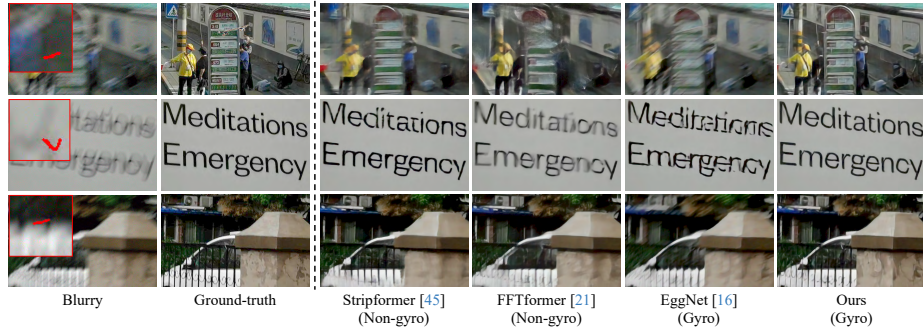


Fig. 6: Qualitative comparison on GyroBlur-Synth. The red curves overlaid on the blurred images visualize the input gyro data.

Comparison with state-of-the-art methods We first compare GyroDeblurNet with state-of-the-art single image deblurring methods that use gyro data [16, 30] and those that do not [3, 21, 45, 47, 51]. We evaluate the performance of all the models on the test set of GyroBlur-Synth with gyro errors. The results are presented in Tab. 1. All the models in the table were trained with GyroBlur-Synth using their own hyperparameter settings.

As shown in Tab. 1, GyroDeblurNet outperforms all the previous non-gyro-based methods by a large margin. Especially compared to Uformer-B [47], Stripformer [45] and FFTformer [21], which adopt transformers, our method requires a significantly smaller amount of computation, and a shorter computation time, while achieving more than 1 dB higher PSNR. Moreover, our method outperforms all the previous gyro-based methods by a large margin, while ours requires a comparable model size and a much smaller computational overhead.

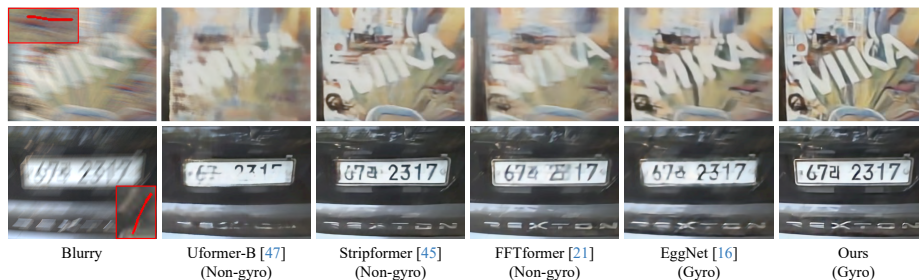


Fig. 7: Qualitative comparison on GyroBlur-Real. The red curves overlaid on the blurred images visualize the input gyro data.

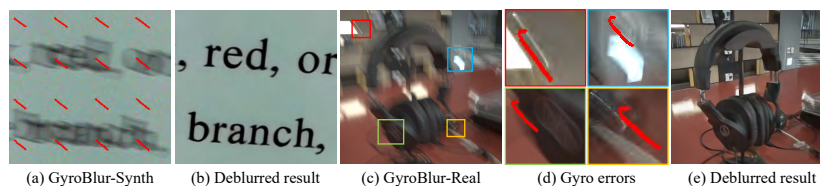


Fig. 8: Camera motion field visualization on a GyroBlur-Synth image and a GyroBlur-Real image. (a) camera motion field visualization on a GyroBlur-Synth image. (b) Our result of (a). (c) A GyroBlur-Real image. (d) Gyro errors. (e) Our result of (c).

Qualitative comparisons on GyroBlur-Synth and GyroBlur-Real are shown in Fig. 6 and in Fig. 7, respectively. As shown in the figures, the previous non-gyro-based methods fail to restore sharp details due to severe blur. Moreover, despite the input gyro data, the previous gyro-based methods also fail to produce sharp details as they are not robust to gyro errors. On the other hand, our method successfully restores sharp images as our method can effectively exploit gyro data with errors.

Gyro errors As discussed in Sec. 1, real-world gyro data cannot accurately represent the camera motion due to gyro noise and missing information such as rotational centers. Fig. 8 shows examples of such gyro errors in our datasets where camera motion fields are visualized as red curves. As shown in the figure, the camera motion information in the camera motion fields in both GyroBlur-Synth and GyroBlur-Real do not perfectly match the blur trajectories in the blurred images due to gyro errors. Nonetheless, GyroDeblurNet successfully restores sharp images for both synthetic and real-world input images.

Effect of training with noisy gyro data

Our training data includes gyro errors to generalize our model to real-world gyro errors. Here we demonstrate the effect of the synthetically added gyro errors. Fig. 9 shows that the model trained with noisy gyro data successfully removes blur from a real-world blurred image with gyro errors, while the one trained with noise-free gyro data fails. Tab. 2 presents a quantitative comparison on GyroBlur-Synth. As shown in the table, training with noisy gyro data substantially im-

Table 2: Results on GyroBlur-Synth with two models trained with noisy and noise-free gyro data.

| Gyro data | Noisy | Noise-free |
|-----------|--------|------------|
| PSNR | 27.28 | 24.94 |
| SSIM | 0.7803 | 0.7112 |



Fig. 9: Effect of training with noisy gyro data. (a) Real-world blurred image. (b) Model trained with noisy gyro data. (c) Model trained with noise-free gyro data.

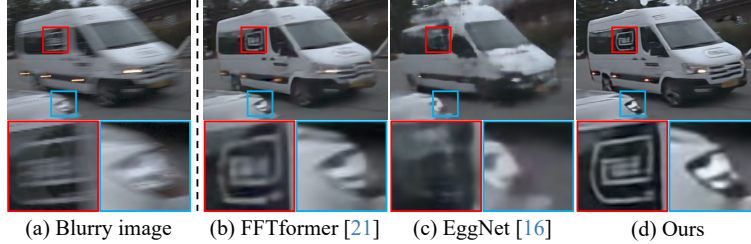


Fig. 10: Results of a real-world blurred image with a moving object.

proves the deblurring quality by more than 2 dB, proving that including gyro errors in the training data is crucial for the training of gyro-based deblurring.

Moving objects Another source of gyro error is moving objects with different blur trajectories as discussed in Sec. 1. Fig. 10 shows a real-world example where the input blurry image has a moving object with different blur trajectory. Due to severe blur, the result of FFTformer [21], the state-of-the-art non-gyro-based method, still has remaining blur in both background and moving object. EggNet [16] also fails to deblur the image as it does not consider neither moving objects nor gyro errors. In contrast, our method successfully restores sharp details both on the moving object and the background thanks to its robustness to gyro errors.

Camera motion field hyperparameter M We investigate the impact of the hyperparameter M that determines the temporal resolution of the camera motion field. To verify the effect of M , we compare the deblurring performance of different values of M . As shown in Tab. 3, the deblurring quality improves gradually as

Table 3: Effect of camera motion field hyperparameter M .

| M | 2 | 4 | 8 | 16 |
|------|--------|--------|--------|--------|
| PSNR | 25.71 | 26.80 | 27.28 | 27.32 |
| SSIM | 0.7706 | 0.7651 | 0.7803 | 0.7811 |

M increases. This highlights the importance of gyro data representation that can capture real-world intricate camera motions, and also explains the limited performance of previous gyro-based approaches [16, 30]. Fig. 11 also demonstrates the effect of increasing the number of vectors to handle complex real-world motion blur. However, increasing M to 16 does not yield a significant performance gain while it doubles the memory consumption, indicating that $M = 8$ is sufficient to represent the camera shakes in most of the images in the test set of GyroBlur-Synth.

Ablation study We conduct an ablation study to investigate the effect of individual components in our method. Specifically, we first study the impact of

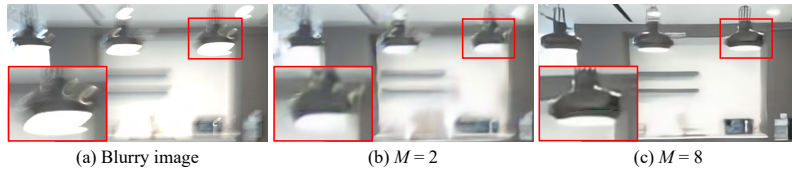


Fig. 11: Effect of increasing M for real-world complex motion blur. (a) Real-world blurry image with complex blur. (b) Result with $M = 2$. (c) Result with $M = 8$.

Table 4: Ablation study on the components of GyroDeblurNet.

| Model | PSNR | SSIM |
|--|-------|--------|
| (a) Deblurring with no gyro data | 24.90 | 0.6997 |
| (b) Gyro refine. w/o image features | 26.64 | 0.7584 |
| (c) Deform. conv. using only gyro features | 26.68 | 0.7588 |
| (d) GyroDeblurNet | 26.94 | 0.7667 |
| (e) GyroDeblurNet + curriculum learning | 27.28 | 0.7803 |

using gyro data. To this end, we build a variant of GyroDeblurNet that has no gyro module, and uses only image features for computing deformable convolution offsets in the gyro deblurring blocks. In our method, we compensate for gyro errors using image features in the gyro refinement and gyro deblurring blocks. Thus, we also examine the effect of using image features in these blocks using two variants of GyroDeblurNet. Specifically, we build one variant without the connections from the image deblurring module to the gyro module, and another variant that computes deformable convolution offsets using only gyro features. We trained all the aforementioned models and our full model without curriculum learning. Finally, to study the impact of the curriculum-learning-based training scheme, we also include our full model trained with curriculum learning.

Tab. 4 reports the comparison result. As shown in Tab. 4 (a), deblurring with no gyro data performs the worst as it cannot benefit from the blur cue provided by gyro data. The results in Tab. 4 (b) and (c) show that exploiting gyro data enhances deblurring quality, but their performances are still worse than our full model in (d) as they do not fully compensate for gyro errors. Finally, the curriculum learning (Tab. 4 (e)) substantially improves the deblurring quality as it helps train the model to fully utilize gyro data.

6 Conclusion

In this paper, we proposed GyroDeblurNet, a novel gyro-based single image deblurring method that can effectively restore sharp images with the help of gyro data. To fully exploit gyro data while considering real-world gyro error, we presented a novel gyro refinement block, a novel gyro deblurring block, and a curriculum learning-based training strategy. In addition, we also presented the camera motion field, a novel gyro embedding scheme to represent real-world camera motions. Finally, we proposed synthetic and real datasets where blurred images are paired with gyro data. Extensive quantitative and qualitative experiments demonstrate the effectiveness of our approach.

Limitations and future work Our method has a few limitations. While our method uses a fixed value for the hyperparameter M , the complexity of camera shakes may increase along with the exposure time, which means that a

longer exposure time may require a larger value for M . Our method does not use the accelerometer, which is also equipped with most smartphones nowadays, and which may provide additional valuable information on the camera motion. Our image deblurring module adopts a relatively simple network architecture compared to recent non-gyro-based single image deblurring approaches, and this may limit the deblurring performance of our method. Extending our work to address these limitations would be an interesting future direction.

References

1. OpenCamera-Sensors. <https://github.com/prime-slam/OpenCamera-Sensors>
2. Bengio, Y., Louradour, J., Collobert, R., Weston, J.: Curriculum learning. In: Proceedings of the 26th annual international conference on machine learning. pp. 41–48 (2009)
3. Chen, L., Chu, X., Zhang, X., Sun, J.: Simple baselines for image restoration. In: European Conference on Computer Vision. pp. 17–33. Springer (2022)
4. Chen, L., Lu, X., Zhang, J., Chu, X., Chen, C.: Hinet: Half instance normalization network for image restoration. In: Proceedings of the IEEE/CVF Conference on Computer Vision and Pattern Recognition. pp. 182–192 (2021)
5. Cho, S.J., Ji, S.W., Hong, J.P., Jung, S.W., Ko, S.J.: Rethinking coarse-to-fine approach in single image deblurring. In: Proceedings of the IEEE/CVF international conference on computer vision. pp. 4641–4650 (2021)
6. Cho, S., Lee, S.: Fast motion deblurring. *ACM Trans. Graph.* **28**(5), 145:1–145:8 (Dec 2009). <https://doi.org/10.1145/1618452.1618491>, <http://doi.acm.org/10.1145/1618452.1618491>
7. Dai, J., Qi, H., Xiong, Y., Li, Y., Zhang, G., Hu, H., Wei, Y.: Deformable convolutional networks. In: Proceedings of the IEEE international conference on computer vision. pp. 764–773 (2017)
8. Deng, S., Ren, W., Yan, Y., Wang, T., Song, F., Cao, X.: Multi-scale separable network for ultra-high-definition video deblurring. In: the IEEE/CVF International Conference on Computer Vision (ICCV). pp. 14030–14039 (2021)
9. Faizullin, M., Kornilova, A., Akhmetyanov, A., Ferrer, G.: Twist-n-sync: Software clock synchronization with microseconds accuracy using mems-gyroscopes. *Sensors* **21**(1) (2021). <https://doi.org/10.3390/s21010068>, <https://www.mdpi.com/1424-8220/21/1/68>
10. Fedasyuk, D., Marusenkova, T.: MemS gyroscopes’ noise simulation algorithm. In: Shakhovska, N., Medykovskyy, M.O. (eds.) *Advances in Intelligent Systems and Computing IV*. pp. 951–967. Springer International Publishing, Cham (2020)
11. Hee Park, S., Levoy, M.: Gyro-based multi-image deconvolution for removing hand-shake blur. In: Proceedings of the IEEE Conference on Computer Vision and Pattern Recognition. pp. 3366–3373 (2014)
12. Hirsch, M., Schuler, C.J., Harmeling, S., Schölkopf, B.: Fast removal of non-uniform camera shake. In: 2011 International Conference on Computer Vision. pp. 463–470. IEEE (2011)
13. Hu, J., Shen, L., Sun, G.: Squeeze-and-excitation networks. In: Proceedings of the IEEE conference on computer vision and pattern recognition. pp. 7132–7141 (2018)
14. Hu, Z., Yuan, L., Lin, S., Yang, M.H.: Image deblurring using smartphone inertial sensors. In: Proceedings of the IEEE Conference on Computer Vision and Pattern Recognition. pp. 1855–1864 (2016)

15. Ji, H., Wang, K.: Robust image deblurring with an inaccurate blur kernel. *IEEE Transactions on Image processing* **21**(4), 1624–1634 (2011)
16. Ji, S., Hong, J.P., Lee, J., Baek, S.J., Ko, S.J.: Robust single image deblurring using gyroscope sensor. *IEEE Access* **9**, 80835–80846 (2021)
17. Joshi, N., Kang, S.B., Zitnick, C.L., Szeliski, R.: Image deblurring using inertial measurement sensors. *ACM Transactions on Graphics (TOG)* **29**(4), 1–9 (2010)
18. Joshi, N., Zitnick, C.L., Szeliski, R., Kriegman, D.J.: Image deblurring and denoising using color priors. In: 2009 IEEE Conference on Computer Vision and Pattern Recognition. pp. 1550–1557. IEEE (2009)
19. Kim, D., M’Closkey, R.T.: Spectral analysis of vibratory gyro noise. *IEEE Sensors Journal* **13**(11), 4361–4374 (2013). <https://doi.org/10.1109/JSEN.2013.2269797>
20. Kingma, D.P., Ba, J.: Adam: A method for stochastic optimization. arXiv preprint arXiv:1412.6980 (2014)
21. Kong, L., Dong, J., Ge, J., Li, M., Pan, J.: Efficient frequency domain-based transformers for high-quality image deblurring. In: Proceedings of the IEEE/CVF Conference on Computer Vision and Pattern Recognition. pp. 5886–5895 (2023)
22. Krishnan, D., Fergus, R.: Fast image deconvolution using hyper-laplacian priors. *Advances in neural information processing systems* **22** (2009)
23. Kupyn, O., Budzan, V., Mykhailych, M., Mishkin, D., Matas, J.: Deblurgan: Blind motion deblurring using conditional adversarial networks. In: Proceedings of the IEEE conference on computer vision and pattern recognition. pp. 8183–8192 (2018)
24. Kupyn, O., Martyniuk, T., Wu, J., Wang, Z.: Deblurgan-v2: Deblurring (orders-of-magnitude) faster and better. In: Proceedings of the IEEE/CVF International Conference on Computer Vision. pp. 8878–8887 (2019)
25. Lee, J., Ji, S.W., Cho, S.J., Hong, J.P., Ko, S.J.: Deep learning-based deblur using gyroscope data. In: 2020 IEEE International Conference on Consumer Electronics-Asia (ICCE-Asia). pp. 1–4. IEEE (2020)
26. Levin, A., Fergus, R., Durand, F., Freeman, W.T.: Image and depth from a conventional camera with a coded aperture. *ACM transactions on graphics (TOG)* **26**(3), 70-es (2007)
27. Lin, T.Y., Maire, M., Belongie, S., Hays, J., Perona, P., Ramanan, D., Dollár, P., Zitnick, C.L.: Microsoft coco: Common objects in context. In: Computer Vision–ECCV 2014: 13th European Conference, Zurich, Switzerland, September 6–12, 2014, Proceedings, Part V 13. pp. 740–755. Springer (2014)
28. Loshchilov, I., Hutter, F.: Sgdr: Stochastic gradient descent with warm restarts. arXiv preprint arXiv:1608.03983 (2016)
29. Mustaniemi, J., Kannala, J., Särkkä, S., Matas, J., Heikkilä, J.: Fast motion deblurring for feature detection and matching using inertial measurements. In: 2018 24th International Conference on Pattern Recognition (ICPR). pp. 3068–3073. IEEE (2018)
30. Mustaniemi, J., Kannala, J., Särkkä, S., Matas, J., Heikkilä, J.: Gyroscope-aided motion deblurring with deep networks. In: 2019 IEEE Winter Conference on Applications of Computer Vision (WACV). pp. 1914–1922. IEEE (2019)
31. Nah, S., Hyun Kim, T., Mu Lee, K.: Deep multi-scale convolutional neural network for dynamic scene deblurring. In: Proceedings of the IEEE conference on computer vision and pattern recognition. pp. 3883–3891 (2017)
32. Pan, J., Hu, Z., Su, Z., Yang, M.H.: Deblurring text images via l0-regularized intensity and gradient prior. In: Proceedings of the IEEE Conference on Computer Vision and Pattern Recognition. pp. 2901–2908 (2014)

33. Richardson, W.H.: Bayesian-based iterative method of image restoration. *JoSA* **62**(1), 55–59 (1972)
34. Rim, J., Kim, G., Kim, J., Lee, J., Lee, S., Cho, S.: Realistic blur synthesis for learning image deblurring. In: *Proceedings of the European Conference on Computer Vision (ECCV)* (2022)
35. Rim, J., Lee, H., Won, J., Cho, S.: Real-world blur dataset for learning and benchmarking deblurring algorithms. In: *Proceedings of the European Conference on Computer Vision (ECCV)* (2020)
36. Ronneberger, O., Fischer, P., Brox, T.: U-net: Convolutional networks for biomedical image segmentation. In: *International Conference on Medical image computing and computer-assisted intervention*. pp. 234–241. Springer (2015)
37. Sangineto, E., Nabi, M., Culibrk, D., Sebe, N.: Self paced deep learning for weakly supervised object detection. *IEEE transactions on pattern analysis and machine intelligence* **41**(3), 712–725 (2018)
38. Schubert, D., Goll, T., Demmel, N., Usenko, V., Stückler, J., Cremers, D.: The tum vi benchmark for evaluating visual-inertial odometry. In: *2018 IEEE/RSJ International Conference on Intelligent Robots and Systems (IROS)*. pp. 1680–1687. IEEE (2018)
39. Shi, M., Ferrari, V.: Weakly supervised object localization using size estimates. In: *Computer Vision–ECCV 2016: 14th European Conference, Amsterdam, The Netherlands, October 11–14, 2016, Proceedings, Part V 14*. pp. 105–121. Springer (2016)
40. Sindelar, O., Sroubek, F.: Image deblurring in smartphone devices using built-in inertial measurement sensors. *Journal of Electronic Imaging* **22**(1), 011003 (2013)
41. Sindelar, O., Sroubek, F., Milanfar, P.: Space-variant image deblurring on smartphones using inertial sensors. In: *Proceedings of the IEEE Conference on Computer Vision and Pattern Recognition Workshops*. pp. 191–192 (2014)
42. Sinha, S., Garg, A., Larochelle, H.: Curriculum by smoothing. *Advances in Neural Information Processing Systems* **33**, 21653–21664 (2020)
43. Tang, X., Zhao, X., Liu, J., Wang, J., Miao, Y., Zeng, T.: Uncertainty-aware unsupervised image deblurring with deep residual prior. In: *Proceedings of the IEEE/CVF Conference on Computer Vision and Pattern Recognition*. pp. 9883–9892 (2023)
44. Tao, X., Gao, H., Shen, X., Wang, J., Jia, J.: Scale-recurrent network for deep image deblurring. In: *Proceedings of the IEEE conference on computer vision and pattern recognition*. pp. 8174–8182 (2018)
45. Tsai, F.J., Peng, Y.T., Lin, Y.Y., Tsai, C.C., Lin, C.W.: Stripformer: Strip transformer for fast image deblurring. In: *ECCV* (2022)
46. Vasu, S., Maligireddy, V.R., Rajagopalan, A.: Non-blind deblurring: Handling kernel uncertainty with cnns. In: *Proceedings of the IEEE Conference on Computer Vision and Pattern Recognition*. pp. 3272–3281 (2018)
47. Wang, Z., Cun, X., Bao, J., Zhou, W., Liu, J., Li, H.: Uformer: A general u-shaped transformer for image restoration. In: *Proceedings of the IEEE/CVF Conference on Computer Vision and Pattern Recognition*. pp. 17683–17693 (2022)
48. Whyte, O., Sivic, J., Zisserman, A., Ponce, J.: Non-uniform deblurring for shaken images. In: *2010 IEEE Computer Society Conference on Computer Vision and Pattern Recognition*. pp. 491–498 (2010). <https://doi.org/10.1109/CVPR.2010.5540175>
49. Wiener, N.: *Extrapolation, interpolation, and smoothing of stationary time series: with engineering applications*. The MIT press (1949)

50. Xu, Y., Zhu, Y., Quan, Y., Ji, H.: Attentive deep network for blind motion deblurring on dynamic scenes. *Computer Vision and Image Understanding* **205**, 103169 (2021)
51. Zamir, S.W., Arora, A., Khan, S., Hayat, M., Khan, F.S., Yang, M.H., Shao, L.: Multi-stage progressive image restoration. In: *Proceedings of the IEEE/CVF conference on computer vision and pattern recognition*. pp. 14821–14831 (2021)
52. Zhang, H., Wipf, D.: Non-uniform camera shake removal using a spatially-adaptive sparse penalty. *Advances in Neural Information Processing Systems* **26** (2013)
53. Zhang, H., Dai, Y., Li, H., Koniusz, P.: Deep stacked hierarchical multi-patch network for image deblurring. In: *Proceedings of the IEEE/CVF Conference on Computer Vision and Pattern Recognition*. pp. 5978–5986 (2019)
54. Zhang, S., Zhen, A., Stevenson, R.L.: A dataset for deep image deblurring aided by inertial sensor data. *Electronic Imaging* **2020**(14), 379–1 (2020)
55. Zhu, X., Hu, H., Lin, S., Dai, J.: Deformable convnets v2: More deformable, better results. In: *Proceedings of the IEEE/CVF conference on computer vision and pattern recognition*. pp. 9308–9316 (2019)